Kinetic and Mechanistic Analysis of the *Escherichia coli ribD*-Encoded Bifunctional Deaminase-Reductase Involved in Riboflavin Biosynthesis[†]

Maria L. B. Magalhães, Argyrides Argyrou,[‡] Sean M. Cahill, and John S. Blanchard*

Department of Biochemistry, Albert Einstein College of Medicine, 1300 Morris Park Avenue, Bronx, New York 10461

Received February 14, 2008; Revised Manuscript Received April 28, 2008

ABSTRACT: Riboflavin is biosynthesized by most microorganisms and plants, while mammals depend entirely on the absorption of this vitamin from the diet to meet their metabolic needs. Therefore, riboflavin biosynthesis appears to be an attractive target for drug design, since appropriate inhibitors of the pathway would selectively target the microorganism. We have cloned and solubly expressed the bifunctional *ribD* gene from *Escherichia coli*, whose three-dimensional structure was recently determined. We have demonstrated that the rate of deamination (370 min^{-1}) exceeds the rate of reduction (19 min^{-1}), suggesting no channeling between the two active sites. The reductive ring opening reaction occurs via a hydride transfer from the C_4-*pro-R* hydrogen of NADPH to C′-1 of ribose and is the rate-limiting step in the overall reaction, exhibiting a primary kinetic isotope effect (^{D}V) of 2.2. We also show that the INH−NADP adduct, one of the active forms of the anti-TB drug isoniazid, inhibits the *E. coli* RibD. On the basis of the observed patterns of inhibition versus the two substrates, we propose that the RibD-catalyzed reduction step follows a kinetic scheme similar to that of its structural homologue, DHFR.

Riboflavin is the direct precursor of flavin mononucleotide (FMN) and flavin adenine dinucleotide (FAD), the redox cofactors found in flavoenzymes, which are involved in a variety of essential cellular processes (*1*). Riboflavin is biosynthetically produced by most prokaryotes, fungi, and plants (*2, 3*). Some microorganisms can also transport riboflavin from the external environment due to the expression of specific membrane transporters (*4, 5*). Conversely, mammals lack the riboflavin biosynthetic pathway and depend entirely on the absorption of this vitamin from the diet. Some pathogenic microorganisms lack an efficient riboflavin uptake system and depend entirely on their ability to produce the vitamin, suggesting that they might be particularly vulnerable to inhibitors of this pathway. Therefore, riboflavin biosynthesis appears to be an attractive target for antimicrobial intervention and drug design, since appropriate inhibitors would selectively target the microorganism, with potentially few side effects in humans.

For this reason, the biosynthesis of riboflavin has been the subject of considerable investigation over the years. The early findings about the nature of the biosynthetic precursor of riboflavin came from the observation that exogenously added purines increased riboflavin production in flavinogenic microorganisms (*6*). Later studies identified guanosine triphosphate (GTP) as the purine precursor, supplying the pyrimidine ring and the ribityl side chain of the vitamin (*2*). In later studies, Bacher and co-workers isolated riboflavin-requiring mutants of *Saccharomyces cerevisiae* and characterized their accumulation products. On the basis of these collective results, they proposed a pathway for the biosynthesis of riboflavin, which is summarized in Figure 1 (*2, 3, 7–9*).

The first step in the pathway involves the hydrolytic opening of the imidazole ring of GTP (**1** in Figure 1) and release of pyrophosphate by GTP cyclohydrolase II (RibA),[1] forming the monophosphorylated pyrimidine derivative, 2,5-diamino-6-ribosylamino-4(3*H*)-pyrimidinone 5′-phosphate (compound **2** in Figure 1) (*10–13*). The product of RibA is converted to 5-amino-6-ribitylamino-2,4(1*H*,3*H*)-pyrimidinone 5′-phosphate (compound **4** in Figure 1), through a sequence of two enzymatic reactions involving deamination of the 2-amino group and reduction of the ribose ring (*14, 15*). Initial studies with cell extracts of *Escherichia coli* suggested that two separate enzymes catalyzed these two reaction steps (*15*). More recently, it has been found that these reactions are, in fact, catalyzed by bifunctional proteins containing an N-terminal deaminase and a C-terminal reductase domain, encoded by the gene termed *ribD* or *ribG* from *E. coli* or *Bacillus subtilis*, respectively (*14*). Since then, a large number of putative orthologs of the bifunctional *ribD* gene have been found in eubacterial genomes.

[†] This work was supported by the National Institutes of Health (NIH) (Grant AI33696 to J.S.B.). The AECOM Structural NMR Resource is supported by the Albert Einstein College of Medicine and in part by grants from the National Science Foundation (DBI9601607 and DBI0331934), the NIH (RR017998), and the HHMI Research Resources for Biomedical Sciences.

* To whom correspondence should be addressed. E-mail: blanchar@aecom.yu.edu. Phone: (718) 430-3096. Fax: (718) 430-8565.

[‡] Present address: Department of Chemical Enzymology, Bristol-Myers-Squibb Pharmaceutical Co., Research & Development, P.O. Box 5400, Princeton, NJ 08543-5400.

[1] Abbreviations: CDA, cytidine deaminase; DMRL, 6,7-dimethyl-8-ribityllumazine phosphate; DHF, dihydrofolate; DHFR, dihydrofolate reductase; Hepes, *N*-(2-hydroxyethyl)piperazine-*N*′-2-ethanesulfonic acid; HGPRTase, hypoxanthine-guanine phosphoribosyltransferase; INH, isoniazid; IPTG, isopropyl thio-β-D-galactopyranoside; PRPPase, 5′-phosphoribosylpyrophosphate synthetase; RibA, GTP cyclohydrolase II; RibD, bifunctional pyrimidine deaminase-reductase; TEA, triethanolamine hydrochloride; THF, tetrahydrofolate.

10.1021/bi800264g CCC: $40.75
Published on Web 05/24/2008

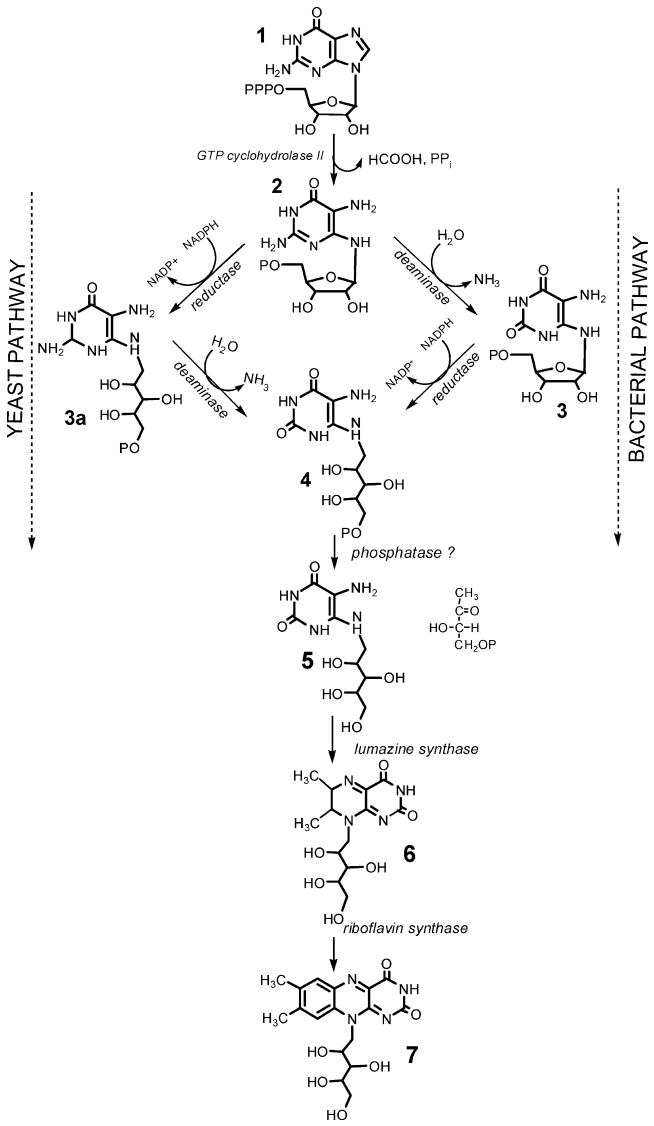

FIGURE 1: Biosynthesis of riboflavin. (**1**) GTP, (**2**) 2,5-diamino-6-ribosylamino-4(3*H*)-pyrimidinone 5′-phosphate, (**3**) 5-amino-6-ribosylamino-4(3*H*)-pyrimidinone 5′-phosphate, (**3a**) 2,5-diamino-6-ribitylamino-2,4(1*H*,3*H*)-pyrimidinone 5′-phosphate, (**4**) 5-amino-6-ribitylamino-2,4(1*H*,3*H*)-pyrimidinone 5′-phosphate, (**5**) 5-amino-6-ribitylamino-2,4(1*H*,3*H*)-pyrimidinone, (**6**) 6,7-dimethyl-8-ribityllumazine, and (**7**) riboflavin.

Previous observations made by Bacher and co-workers on the excretion products of riboflavin-requiring mutants of *S. cerevisae* suggested that reduction precedes deamination in yeasts (*8*). These findings were later confirmed by in vitro studies with the *Ashbya gossypii* (*16*) and *Candida guilliermondii* enzymes (*17*). Conversely, studies performed in bacteria suggested that deamination of the pyrimidine ring precedes reduction of the ribose moiety, and it was concluded that the pathway is different in bacteria and yeasts (*15*). More recently, Bacher and co-workers demonstrated that the product of gene At4g20960 in *Arabidopis thaliana* catalyzes deamination of compound **2** (*18*). ^{13}C NMR analysis demonstrated that the enzyme product is identical to that obtained from the bifunctional *E. coli* RibD. These studies support the proposal that the deamination and reduction steps in plants and bacteria proceed by a different order compared to that in fungi.

Although the crystal structures of the bifunctional deaminase-reductase from *E. coli* and *B. subtilis* have been recently reported (*19, 20*), little is known about the detailed kinetic and chemical mechanisms of RibD, and this is the least studied enzyme in the pathway. The paucity of studies with this enzyme is likely due to the fact that RibD is an extremely slow turnover enzyme with a chemically unstable substrate, intermediate, and product, all of which are neither commercially available nor easily detected.

The crystal structure of the *B. subtilis* enzyme showed that the deaminase active site contains a tightly bound zinc ion and displays a high degree of structural homology to the cytidine deaminase (CDA) superfamily (*20*). Members of the CDA superfamily have a virtually identical zinc-dependent deamination mechanism, with consensus histidine and cysteine residues acting as the zinc ligands. The C-terminal reductase domain displays significant structural similarity to dihydrofolate reductases (DHFRs), sharing an almost identical binding architecture for NADPH binding (*19, 20*). The available structures also reveal that the deaminase and reductase functional domains are independent, with no obvious channel connecting the two active sites.

The chemical mechanism of the NADPH-dependent ribose ring reduction was investigated by in vivo experiments with the yeast *A. gossypii* (*21*). Evidence suggested that reduction of the ribosyl moiety occurred by hydride transfer to C-1′ of the ribose ring. On the basis of this finding, the authors proposed that catalysis occurred by proton abstraction at the amine nitrogen next to C-1′, forming a Schiff base intermediate, followed by hydride transfer from NADPH to C-1′ (Figure 2). Studies with riboflavin-requiring mutants of *B. subtilis*, however, showed the accumulation of an Amadori derivative, suggesting that in bacteria, the reaction would occur through the formation of an Amadori intermediate followed by reduction at C-2′ (Figure 2) (*22*). To date, no evidence supporting the location of hydride transfer has been provided for a eubacterial bifunctional deaminase-reductase.

MATERIALS AND METHODS

Cloning and Expression of the E. coli ribA and ribD Genes. The synthetic oligonucleotide primers (5′-GCATATGCAGGACGAGTATTACAT-3′ and 5′-GAAGCTTCATGCACCCACTAAATGCA-3′ and 5′-CGCCATATGCAGCTTAAACGTGTGGCAGAAGCC-3′ and 5′-CGCAAGCTTTTATTTGTTCAGCAAATGGCCC-3′) were used to amplify the *E. coli ribD* and *ribA* genes, respectively, from *E. coli* genomic DNA using standard PCR conditions. The primers were complementary to the 5′ and 3′ ends of the *ribD* and *ribA* genes and introduced unique *Nde*I and *Hin*dIII restriction enzyme sites. The blunt PCR products were ligated into the pCR-Blunt cloning vector (Invitrogen). The recombinant vectors were digested with *Nde*I and *Hin*dIII restriction enzymes, and the released gene products were ligated into pET28a(+) expression vectors, previously digested with the same enzymes. The pET28a(+) expression vector carries an N-terminal six-His tag which allows for affinity column purification procedures. The recombinant plasmids pET28a(+)::*ribD* and pET28a(+)::*ribA* were sequenced, confirming both their identity and the lack of spurious mutations. *E. coli* BL21(DE3) cells were transformed with either pET28a(+)::*ribD or* pET28a(+)::*ribA*, inoculated into LB medium containing 50 μg/mL kanamycin, and induced at 37 °C with 0.3 mM IPTG for 12 h. Protein expression was analyzed by SDS−PAGE.

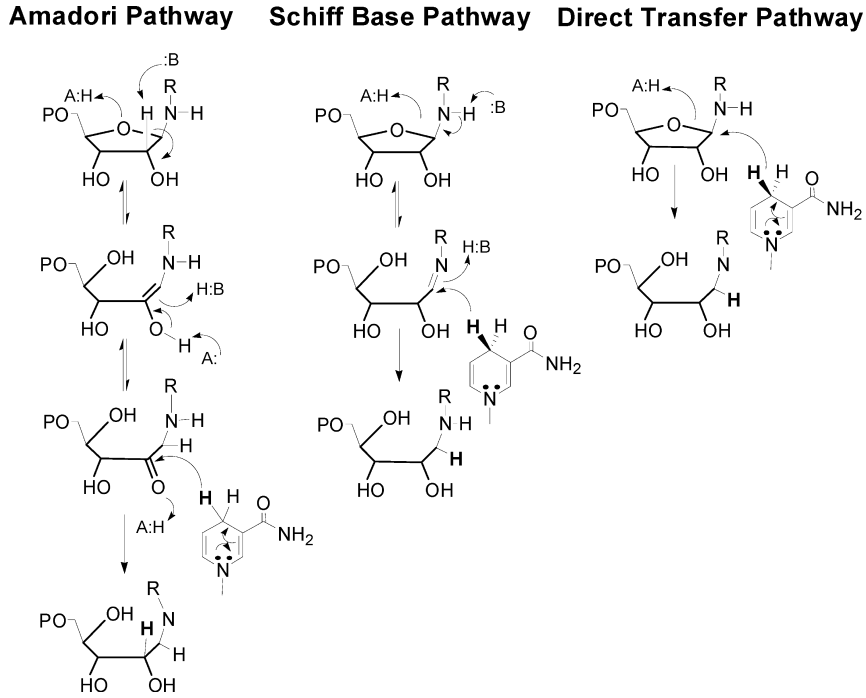

FIGURE 2: Proposed mechanisms for reduction of the ribosylamino to the ribitylamino moiety catalyzed by the reductase domain of RibD.

Site-Directed Mutagenesis of the RibD Deaminase Domain. Abolition of the deaminase activity was achieved by the simultaneous mutation of two cysteine residues involved in zinc coordination (Cys84Ala and Cys75Ala) and one arginine residue possibly involved in substrate binding (Arg80Asp) (*20*). Mutations were introduced into plasmid pET28a(+)::*ribD* using the QuikChange XL site-directed mutagenesis kit (Stratagene), where a specific overlapping primer pair contained all three amino acid mutations (bold and underlined below): 5′-GAACCC**GC**TAGCCATCATG-GT**GA**TACGCCACCG**GC**CTGTGACG-3′ and 5′-CGTCA-C A G **G C** C G G T G G C G T A **T C** A C C A T G A T G-GCTA**GC**GGGTTC-3′). The presence of the desired mutations and the absence of unwanted additional mutations were confirmed by DNA sequencing.

Purification of RibA and RibD. All protein purification procedures described here were carried out at 4 °C, and protein purity was analyzed by SDS−PAGE on a Phast System (Pharmacia). *E. coli* cells harboring either pET28a-(+)::*ribA* or pET28a(+)::*ribD* were suspended in 50 mL of 20 mM triethanolamine hydrochloride (TEA) (pH 7.5) and 10 mM imidazole (buffer A), containing protease inhibitor cocktail (Roche) and DNase I (5 μg/mL). The cells were disrupted by sonication and stirred on ice for 30 min. The cell debris was removed by centrifugation for 45 min at 11000 rpm. The clear soluble fraction was loaded onto a 50 mL nickel-NTA column pre-equilibrated with buffer A, and proteins were eluted with a linear 10 to 500 mM imidazole gradient. Active fractions were pooled, concentrated, and dialyzed against 8 L of 20 mM TEA and 100 mM NaCl (pH 7.5) and stored at −20 °C.

Enzymatic Synthesis of 2,5-Diamino-6-ribosylamino-4(3H)-pyrimidinone 5′-Phosphate (compound **2***).* The reaction mixture for the synthesis of compound **2** contained 50 mM Hepes (pH 8.0), 5 mM $MgCl_2$, and 20 mM GTP (**1**), and the reaction was initiated by the addition of 100 μM RibA. The reaction mixture was incubated at 37 °C for 40 min. We have observed the formation of approximately 10% GMP as a byproduct, as previously described (*11, 12*). We also observed significant degradation of compound **2** after longer periods of reaction. The half-life of compound **2** was measured on the basis of its UV−visible spectroscopic signal and determined to be 9 h. The enzyme was removed by filtering the sample through a 10 kDa cutoff membrane, and aliquots of the sample were immediately flash-frozen (−80 °C) to prevent degradation. Compound **2** was not further purified and stored at −80 °C.

Measurement of Enzyme Activity. The deaminase reaction was monitored by following the disappearance of compound **2** by HPLC analysis. The assay mixtures contained 50 mM Hepes (pH 7.5), 300 nM RibD, and different concentrations of compound **2** (based on HPLC analysis; see below). Initial rates of deamination at each concentration of compound **2** were determined by incubating the reaction mixture at 25 °C for specific periods of time. The reaction was quenched at each time point by passing the sample through a 10 kDa membrane to remove the enzyme and immediately flash-frozen to prevent degradation. Compound **2** was purified by HPLC using an analytical column (Jupiter 5 μM, C18, 300A) and the following program: 0% B from 0 to 2 min, 40% B from 2 to 30 min, 90% B from 30 to 45 min, and 100% B from 45 to 46 min [where A consists of 10 mM tetrabutylammonium hydroxide, 10 mM KH_2PO_4, and 1% methanol (pH 7.0), and B consists of 2.8 mM tetrabutylammonium hydroxide, 100 mM KH_2PO_4, and 30% methanol (pH 5.0)]. The compound was eluted as a double peak at 10 min. The concentration of **2** at each different time point was determined by comparing the peak integration of each HPLC run with a calibration curve (peak area vs concentration) previously established. To perform the calibration curve, compound **2** concentrations were determined by verifying the amount of GTP consumed by HPLC analysis, taking into

account that formation of **2** accounts for only 90% of the RibA products (*11, 12*).

The decrease in the concentration of compound **2** observed was plotted as [compound **2**] versus time to obtain an initial rate. Initial rates were linearly dependent on the concentration of enzyme, and no consumption of **2** was observed in the absence of enzyme. Initial velocities for the reductase reaction of RibD were determined by following the decrease in absorbance at 340 nm, indicative of NADPH oxidation ($\varepsilon_{340} = 6220\ M^{-1}\ cm^{-1}$). A typical reaction mix contained 50 mM Hepes (pH 7.5), 300 nM RibD, and variable concentrations of compound **2** and NADPH. Individual substrate saturation kinetic data were fitted to eq 1

$$v = (VA)/(K_a + A) \quad (1)$$

where v is the measured reaction velocity, V is the maximal velocity, A is the concentration of substrate A, and K_a is the corresponding Michaelis−Menten constant.

Synthesis and Purification of [4R-4-^{2}H]NADPH. The reaction mixture for the synthesis of [4*R*-4-^{2}H]NADPH contained 50 mM Hepes (pH 8.0), 23 mg of $NADP^+$, 180 mg of [1-^{2}H]glucose, and 100 mg of glucose dehydrogenase from *Thermoplasma acidophilum* (*23*) in a 5 mL final volume and was incubated at 37 °C for 1 h. [4*R*-4-^{2}H]NADPH was purified on a Mono Q column (Amersham Biosciences) as previously described (*24*), and the fractions with an A_{260}/A_{340} absorbance ratio of 2.3 were pooled.

Synthesis and Purification of [1′-^{13}C]GTP. [2-^{13}C]-D-Glucose was purchased from Sigma. Hypoxanthine-guanine phosphoribosyltransferase (HGPRTase) and 5′-phosphoribosylpyrophosphate synthetase (PRPPase) were a kind gift from V. L. Schramm. All other enzymes were purchased from Sigma. The reaction mixture for the synthesis of labeled GTP from glucose contained 100 mM potassium phosphate buffer (pH 7.5), 50 mM glycylglycine (pH 8.0), 5 mM $MgCl_2$, 2.5 mM DTT, 40 mM PEP, 0.5 mM ATP, 20 mM α-ketoglutarate, 0.1 mM $NADP^+$, 1 mM [2-^{13}C]-D-glucose, and 1 mM guanine in a reaction volume of 15 mL. To the reaction mixture were added 8 units of pyruvate kinase, 4.5 units of myokinase, 5 units of hexokinase, 5 units of phosphoriboisomerase, 4 units of glucose-6-phosphate dehydrogenase, 5 units of glutamate dehydrogenase, 5 units of phosphogluconic acid dehydrogenase, 1 unit of guanylate kinase, and 0.4 unit of HGPRTase and PRPPase. The reaction was initiated by adding glucose. To overcome guanine insolubility problems, 4 mg of guanine was dissolved in 200 μL of 13 N ammonium hydroxide. Every 4 h, 50 μL aliquots of this guanine solution were added to the 15 mL reaction mixture, and the pH of the reaction mixture was adjusted to pH 7.5. The reaction mixture was incubated for 24 h at 37 °C, and GTP was purified by FPLC on a Mono-Q column using a 20 to 600 mM ammonium bicarbonate gradient for elution. The chromatography was followed at 260 nm, and the pooled fractions were lyophilized.

Synthesis and Purification of DMRL. The reaction mixture for the synthesis of DMRL contained 50 mM Hepes (pH 7.9), 5 mM $MgCl_2$, 4.5 mM [1′-^{13}C]GTP, 100 μM RibA, 200 μM NADPH, 10 mM glucose 6-phosphate, 4 units of glucose-6-phosphate dehydrogenase, and 80 μM RibD in a final volume of 500 μL and was incubated at 37 °C for 1.5 h. 2,3-Butanedione (final concentration of 40 mM) was added for 30 min to convert the deaminated−reduced product of RibD to the stable lumazine derivative. The sample was filtered through a 10 kDa membrane to remove the enzymes and loaded onto an FPLC-MonoQ column. DMRL was followed at 400 nm and eluted using a linear gradient of 20 to 600 mM ammonium bicarbonate. The pooled fractions were lyophilized and stored at −20 °C.

Synthesis and Purification of [1′-^{13}C,1′-^{2}H]DMRL. The reaction mixture for the synthesis of [1′-^{13}C,1′-^{2}H]DMRL contained 50 mM Hepes (pH 7.9), 5 mM $MgCl_2$, 4.5 mM [1′-^{13}C]GTP, 100 μM RibA, 200 μM [4*R*-4-^{2}H]NADPH, 10 mM [1-^{2}H]glucose, 10 units of glucose dehydrogenase from *T. acidophilum*, and 260 μM RibD in a final volume of 500 μL and was incubated at 37 °C for 1.5 h. 2,3-Butanedione (final concentration of 40 mM) was added for 30 min. Purification procedures were performed as described for DMRL.

Primary Kinetic Isotope Effects. The primary kinetic isotope effects on the RibD-catalyzed reduction were determined by direct comparison of the initial velocities using saturating concentrations of compound **2** and variable concentrations of either NADPH or [4*R*-4-^{2}H]NADPH. The kinetic isotope effects were fitted to eq 2

$$v = (VA)/[K_a(1 + F_i E_{V/K}) + A(1 + F_i E_V)] \quad (2)$$

where v is the measured reaction velocity, V is the maximal velocity, A is the concentration of substrate A, K_a is the corresponding Michaelis−Menten constant, $E_{V/K}$ and E_V are the isotope effects minus 1 on V/K and V, respectively, and F_i is the fraction of isotopic label.

Solvent Kinetic Isotope Effects. The solvent kinetic isotope effects on k_{cat} and k_{cat}/K_m were determined by measuring the initial velocities using saturating concentrations of compound **2** and variable concentrations of NADPH in either H_2O or 90% D_2O at pH 7.8.

Bisubstrate Analogue Inhibition of the RibD Reductase Domain. The synthesis and purification of the INH−NADP adduct have been previously described (*25*). Bisubstrate analogue inhibition patterns for the INH−NADP adduct were determined by measuring initial velocities at different concentrations of one reactant, a fixed concentration of the second reactant, and different concentrations of the INH−NADP adduct. First, NADPH concentrations were varied (8, 10, 12, and 16 μM), and the compound **3** concentration was held at 25 or 50 μM. Three different concentrations of the INH−NADP adduct were tested (0, 5, and 10 μM), and the data were fitted to eq 3, which describes linear, competitive inhibition. Bisubstrate inhibition patterns were also determined by varying the concentration of compound **3** (33, 40, 50, 66, and 100 μM) using NADPH at a fixed concentration of 20 μM. Four different concentrations of the INH−NADP inhibitor were tested (0, 10, 20, and 30 μM), and the data were fitted to eq 4, which describes linear, uncompetitive inhibition.

$$v = (V[A])/[K_a(1 + [I_{A-B}]/K_{is}) + [A]] \quad (3)$$

$$v = (V[A])/[K_a + [A](1 + [I_{A-B}]/K_{ii})] \quad (4)$$

where v is the measured initial velocity, V is the maximal velocity, [A] is the concentration of the varied substrate, K_a is the corresponding Michaelis−Menten constant, $[I_{A-B}]$ is the concentration of the bisubstrate inhibitor, and K_{is} and K_{ii} are the slope and intercept inhibition constants, respectively.

NMR Analysis. ^{1}H-decoupled ^{13}C NMR analysis of DMRL was performed on a Bruker DRX300 NMR spectrometer at 25 °C. Simultaneous ^{1}H and ^{2}H decoupling ^{13}C NMR experiments were performed at 25 °C on a Varian Inova 600 MHz spectrometer equipped with a triple-resonance HCN cryoprobe. One-dimensional (1D) ^{13}C spectra were collected using continuous proton waltz decoupling with 50000 scans, a 250 ppm sweep width centered at 90 ppm and sampled with 4096 points, and a recycle delay of 1 s. Spectra were processed with an exponential line broadening of 1 Hz, and the carbon chemical shifts were referenced to 3-(trimethylsilyl)propionate. Some 1D ^{13}C spectra were collected using both continuous proton waltz decoupling and deuterium waltz decoupling gated on during the acquisition period.

RESULTS AND DISCUSSION

To study the kinetic and chemical mechanisms of deamination and reduction reactions catalyzed by the bifunctional RibD, we proposed to isolate the individual reactions. It had been demonstrated that partial expression of either the N-terminal or C-terminal domains of the *B. subtilis* RibG generated active enzymes with very poor enzyme stability (*14*). For this reason, we have studied the full-length RibD in which either the deaminase activity was knocked out by site-directed mutagenesis or the reductase domain was silent due to the absence of NADPH.

We have mutated residues in the deaminase domain by site-directed mutagenesis of two cysteine residues involved in zinc coordination (C84A and C75A) and one residue proposed to be involved in substrate binding (R80D) (*20*). The deaminase mutant enzyme form failed to either deaminate (by HPLC analysis) or reduce compound **2** (by NADPH oxidation), confirming the previously determined order of bacterial pathway, where deamination must precede reduction. To test whether the deaminase-negative enzyme contained a functional reductase domain, we synthesized compound **3** by incubating wild-type RibD with compound **2** in the absence of NADPH. The enzyme was removed by rapidly filtering the sample through a 10 kDa membrane and then immediately adding NADPH and the deaminase mutant to the flow-through. The deaminase-negative enzyme was able to reduce the ribosyl moiety of the preformed **3**, confirming we have produced a full-length RibD with inactive deaminase and active reductase domains.

We next investigated the rate of the individual deaminase reaction. We measured the deaminase activity by incubating compound **2** with RibD in the absence of NADPH and monitored the disappearance of **2** by HPLC analysis. The enzymatic measurements of deamination are described in detail in Materials and Methods. Compound **2** was eluted from the C18-Jupiter column as a double peak at 10 min. Previous studies have shown that RibA produces β-compound **2**, which isomerizes into an equilibrium mixture of the α-isomer spontaneously (*11*). The initial rates of deamination (<20% conversion) were plotted versus the corrected concentration of **2** (Figure 4), and the data were fitted to eq 1. The calculated kinetic parameters indicated that deamination occurs with a k_{cat} of 370 ± 30 min^{-1} with a K_m value of 1.3 ± 0.2 mM. We have determined compound **2** concentrations indirectly on the basis of the amount of GTP consumed by the RibA reaction, and this may not reflect the true amounts of compound **2** due to degradation. Since RibA produces GMP as a 10% byproduct, we tested GMP as a potential inhibitor of both the deaminase and reductase activities. GMP failed to inhibit either activity.

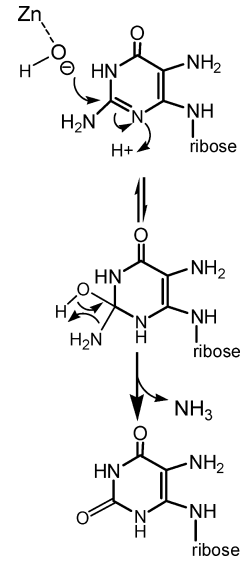

FIGURE 3: Proposed mechanism of deamination.

The deaminase domain displays a high degree of structural homology to the members of the CDA superfamily (*20*). The members of this family catalyze the hydrolytic deamination of nucleotides and share a nearly identical mechanism, in which a zinc-activated water molecule attacks C-2, producing a predicted sp^3-hybridized tetrahedral intermediate, which collapses releasing ammonia and producing the pyrimidinone product (Figure 3) (*26*). It has been shown that analogues mimicking this tetrahedral intermediate are powerful inhibitors of nucleoside deaminases (*27, 28*). For instance, adenosine deaminase was found to be strongly inhibited by nebularine, an sp^3-hybridized analogue with an apparent K_i value of 3×10^{-13} M (*28–30*). In this molecule, a hydrogen atom takes the place of the leaving amine group, and thus, hydrolysis cannot occur. The nonhydrolyzable intermediate may approach the transition-state structure, binding tightly in the enzyme active site and accounting for such extremely high affinity.

On the basis of this rationale, we synthesized a potential substrate for the deaminase domain, where the 2-amino group is replaced with a hydrogen atom, namely 5-amino-6-ribosylamino-4(3*H*)-pyrimidinone 5′-phosphate. If the enzyme accepts this analogue as a substrate and the enzymatic hydration of the analogue results in the formation of the sp^3-hybridized alcohol, the product of the reaction could potentially bind strongly and resist dissociation. To synthesize this molecule, we incubated RibA with ITP, which differs from GTP only in the absence of the 2-amino group. The production of 5-amino-6-ribosylamino-4(3*H*)-pyrimidinone 5′-phosphate was monitored by HPLC analysis. ITP is a substrate for RibA, and the enzyme product is significantly more stable than compound **2**, based on UV spectroscopic analysis. Unfortunately, the compound had no activity with or against the deaminase, presumably because it is not a substrate due to the strict requirement for the 2-amino group for binding. The compound was also tested as an alternative substrate for the reductase domain. Unfortunately, the reductase domain also does not accept 5-amino-6-ribosy-

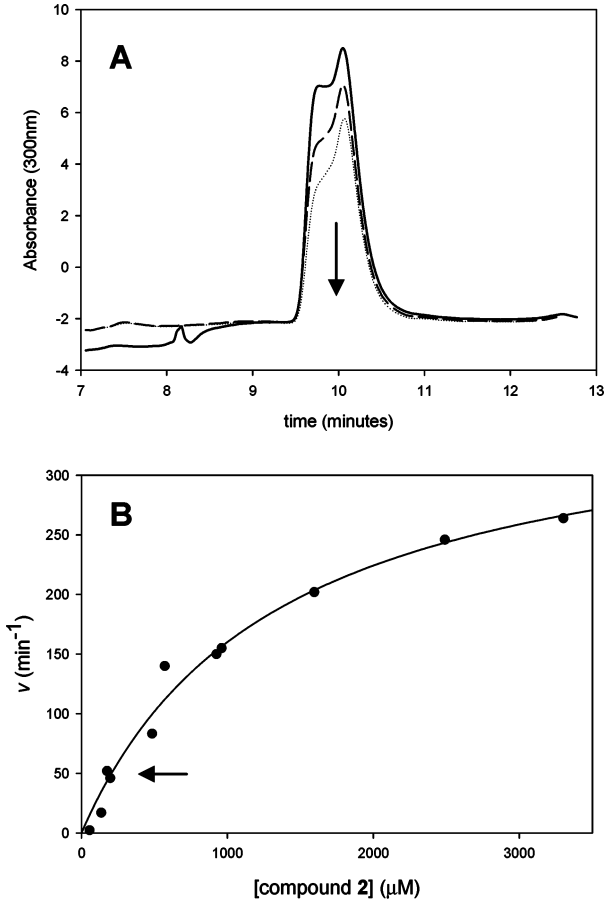

FIGURE 4: Kinetic parameters of the deaminase reaction. (A) HPLC traces of compound **2** consumption using 200 μM compound **2** at 2 (—), 4 (– – –), and 6 min (•••). (B) Saturation curve of the deaminase reaction. Each symbol (●) is the initial rate of deamination at a specific compound **2** concentration, while the line is the fit of the data to eq 1. The arrow indicates the initial rate of deamination using 200 μM compound **2**, the HPLC trace of which is shown in panel A.

lamino-4(3*H*)-pyrimidinone 5′-phosphate as a substrate. Perhaps this is less surprising given the fact that the reductase domain can discriminate unambiguously between the amino and keto groups of compounds **2** and **3**, respectively.

We next focused on the kinetic mechanism of the RibD reductase domain. Reduction was followed by monitoring NAD(P)H oxidation at 340 nm. Kinetic studies were performed using compound **3** preformed in situ, by incubating RibD with compound **2** prior to initiation of the reaction. Reactions were initiated by the addition of NADPH, and the kinetic parameters are summarized in Table 1. The calculated kinetic parameters show that reduction occurs with a k_{cat} of 19 ± 1 min^{-1}, 20 times slower than deamination, indicating that reduction is the second and rate-limiting step in the overall reaction. These results also suggest that the deaminase and reductase activities are not kinetically coupled, which is consistent with the lack of any obvious channel or enzyme surface path connecting the two active sites (*19, 20*).

The crystal structure of the *E. coli* RibD reported short hydrogen bonding interactions between the adenosyl ribose 2′-phosphate of NADPH and residues Ser 234 and Ser 194 (*19*). Our kinetic data indicate that the nonphosphorylated form of the pyrimidine nucleotide, NADH, is an extremely poor substrate, and although the interactions described above

Table 1: Kinetic Parameters for the Deaminase and Reductase Reactions Catalyzed by RibD

substrate	k_{cat} (min^{-1})	K_m (μM)
	Reductase	
compound **3**[a]	19 ± 1	37 ± 5
NADPH[b]	18.5 ± 0.5	20 ± 4
NADH[b]	1.5 ± 0.1	80 ± 20
	Deaminase	
compound **2**[c]	370 ± 30	1300 ± 200

[a] Measured using a fixed concentration of 200 μM NADPH. [b] Measured using a fixed concentration of 800 μM compound **2**. [c] Measured in the absence of NADPH.

Table 2: Bisubstrate Inhibition Constants

varied substrate	inhibition pattern	K_m (μM)	K_{ii} (μM)	K_{is} (μM)
NADPH[a]	competitive	7 ± 2		2.5 ± 0.5
NADPH[b]	competitive	5 ± 4		5 ± 2
compound **3**	uncompetitive	100 ± 8	12 ± 1	

[a] Measured using a fixed concentration of 25 μM compound **3**. [b] Measured using a fixed concentration of 50 μM compound **3**.

do not appear to be essential for catalysis, we believe they are critical for a reduced level of nucleotide binding (Table 1).

The *Mycobacterium tuberculosis* RibG enzyme comprises only the reductase domain of the bifunctional RibD and was recently found to bind the isoniazid−NADP (INH−NADP) adduct in TB extracts (*25*). In this study, we have tested INH−NADP as a bisubstrate analogue inhibitor of the bifunctional *E. coli* RibD. The compound inhibits RibD in the low micromolar range, and the apparent K_i is dependent on the concentration of the second substrate (compound **3**) (see Table 2), which is consistent with the adduct acting as a bisubstrate inhibitor. The bisubstrate inhibitor showed competitive inhibition against NADPH (Figure S1, A) and uncompetitive inhibition versus compound **3** (Figure S1, B). The observed uncompetitive pattern of inhibition versus compound **3** suggests that the inhibitor is binding to one of the enzyme−product complexes. We have considered the chemical and structural similarity between RibD and DHFR in an effort to analyze and interpret these data.

The steady-state kinetic mechanism of *E. coli* DHFR has been determined. In the first catalytic cycle, NADPH and dihydrofolate (DHF) bind to generate the catalytic complex. After hydride transfer to generate the product complex, $NADP^+$ is released and NADPH binds. Tetrahydrofolate (THF) release is rate-limiting, and the binding of NADPH has been proposed to enhance the dissociation of THF (*31, 32*). On the basis of this mechanism, and our observation of competitive inhibition by INH−NADP versus NADPH and uncompetitive inhibition versus compound **3**, we propose a kinetic mechanism similar to that of DHFR (Scheme 1). In the first catalytic cycle, NADPH binds the free enzyme followed by binding of compound **3** to generate the E−NADPH−**3** complex. After hydride transfer, nucleotide exchange takes place ($NADP^+$ release, NADPH binding), followed by release of compound **4** to generate the E−NADPH complex, which then continues under steady-state conditions without any free enzyme. The competitive inhibition by the bisubstrate analogue suggests that it binds to the E−**4** product complex. If this is true, then theory

Scheme 1

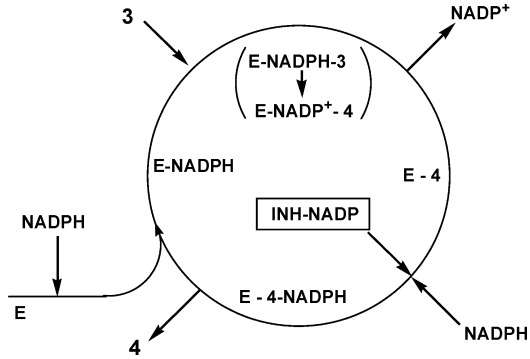

predicts that the inhibition pattern versus compound **3** would be uncompetitive since **4** is released before **3** binds, and this is an irreversible step under initial velocity conditions (*33, 34*). It is unlikely that the release of compound **4** is rate-limiting in the case of RibD, since the observed primary deuterium kinetic isotope effect on the maximal velocity is substantial.

In the reaction catalyzed by DHFR, the *pro-R* hydrogen atom has been shown to be directly transferred to C-6 of dihydrofolate (*32*). The comparison of NADPH binding in the RibD and DHFR active sites showed that the nicotinamide ring binds in essentially the same position in both enzymes (*19*). We therefore investigated the stereochemistry of hydride transfer by probing the kinetic isotope effects using NADPH deuterated at the *pro-R* position. Kinetic isotope effects were determined by direct comparison of the enzymatic rates using either NADPH or [4*R*-4-^{2}H]NADPH as the substrate. The magnitude of the observed kinetic isotope effect ^DV of 2.2 ± 0.4 (Figure 6) is only compatible with this being a primary kinetic isotope effect, and thus, RibD transfers the *pro-R* hydrogen from C-4 of NADPH to

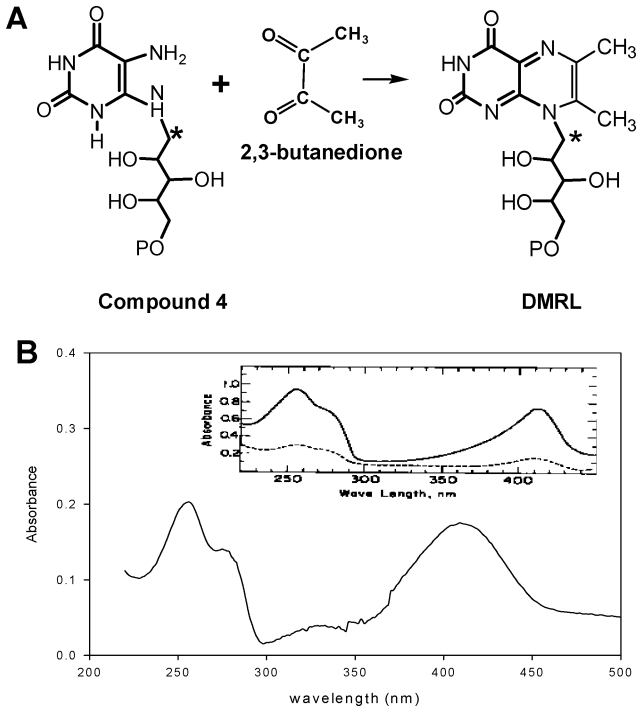

FIGURE 5: Chemical synthesis of [1′-^{13}C]DMRL. (A) Chemical conversion of compound **4** to DMRL in the presence of 2,3-butanedione. (B) Absorption spectra of the produced compound and the authentic DMRL (inset) (*15*). The asterisk indicates ^{13}C labeling at C-1′.

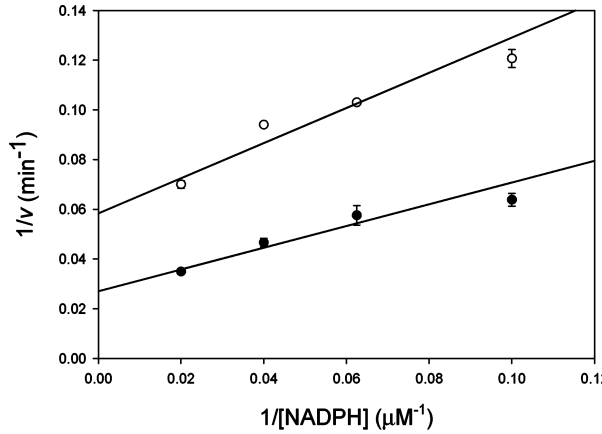

FIGURE 6: Primary deuterium kinetic isotope effects exhibited by RibD using [4*R*-^{2}H]NADPH. The symbols are the experimentally determined values using NADPH (●) or [4*R*-^{2}H]NADPH (○), while the lines are fits of the data to eq 2. NADPH was the variable substrate, and compound **2** was present at nonsaturating concentrations.

compound **3**. The magnitude of the effect also suggests that hydride transfer is potentially the slow step in the reductase reaction, and given the fact that deamination is faster than reduction, we can conclude that, in vitro, hydride transfer is the rate-limiting step on the overall bifunctional reaction.

Additionally, ^DV (2.2) is larger than $^DV/K$ (1.6), suggesting that NADPH is a sticky substrate, dissociating with a rate similar to or slower than that of the catalytic step. NADPH also behaves as a sticky substrate for *E. coli* DHFR (*35*), suggesting that both enzymes share the same binding properties for the pyrimidine nucleotide (*19*).

Although studies in bacteria using riboflavin-requiring mutants of *B. subtilis* showed the accumulation of an Amadori derivative, more recent studies of the mechanism of reductive ring opening using the *A. gossypii* enzyme (*21, 22*) definitively ruled out an Amadori pathway in yeasts. On the basis of these findings, the authors suggested that the yeast enzyme utilizes a Schiff base pathway for reduction of the ribosylamino linkage. To examine the mechanism of reduction by the *E. coli* bifunctional enzyme, we elected to use our knowledge of the stereospecificity of the hydride transfer step.

Our approach was based on the use of [1′-^{13}C]compound **2**, followed by ^{13}C NMR analysis of the enzyme product to investigate the location of hydride transfer. We have synthesized [1′-^{13}C]compound **2** from [1′-^{13}C]GTP, whose synthesis is described in detail in Materials and Methods (Figure S4). [1′-^{13}C]Compound **2** was incubated with RibD in the presence of NADPH to produce the final enzyme product, compound **4**. Orthodiamino pyrimidine compounds, like compound **4**, are quite unstable in aqueous solution. To overcome this issue, and allow for NMR analysis, we have reacted compound **4** with 2,3-butanedione to produce 6,7-dimethyl-8-ribityllumazine phosphate (DMRL), a stable green fluorescent compound (Figure 5A). DMRL was purified by anion-exchange chromatography using a Mono-Q column, and the absorbance at 400 nm was monitored. The compound exhibits an intense green fluorescence under UV light and produces an absorption spectrum identical to that of authentic DMRL (Figure 5B) (*15*). Mass spectrometry analysis of DMRL revealed a mass of 407 Da, which

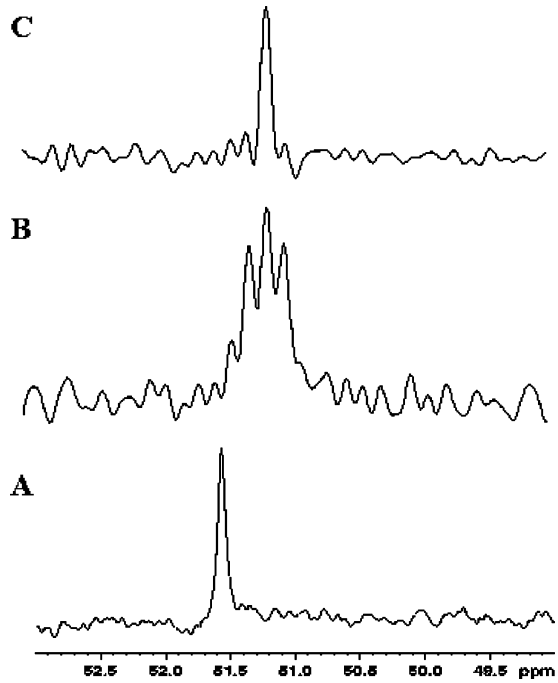

FIGURE 7: Sections of ^{13}C NMR spectra of DMRL: (A) proton-decoupled ^{13}C NMR spectrum of [1′-^{1}H,1′-^{13}C]DMRL, (B) proton-decoupled ^{13}C NMR spectrum of [1′-^{2}H,1′-^{13}C]DMRL, and (C) proton- and deuterium-decoupled ^{13}C NMR spectrum of [1′-^{2}H,1′-^{13}C]DMRL.

confirms the stoichiometric retention of ^{13}C from [1′-^{13}C]GTP in the molecule. The proton-decoupled ^{13}C NMR spectrum of [1′-^{13}C,1′-^{1}H]DMRL (produced using NADPH) revealed a single peak at 51.5 ppm (Figure 7A), in agreement with the resonance assignment previously reported for C-1′ of DMRL (*36*). If the reduced pyridine nucleotide hydride is transferred to C-1′, then [4*R*-4-^{2}H]NADPH should transfer a deuterium atom to C-1′ and the proton-decoupled ^{13}C NMR spectrum should show a triplet due to scalar coupling of a single deuterium atom attached to the carbon nucleus. We enzymatically synthesized [1′-^{13}C,1′-^{2}H]DMRL from [1′-^{13}C]compound **2** and [4*R*-4-^{2}H]NADPH. Mass spectrometric analysis confirmed the incorporation of a deuterium atom by measurement of a mass of 408 Da. As one can see in Figure 7B, the proton-decoupled ^{13}C spectrum of [1′-^{13}C,1′-^{2}H]DMRL revealed a triplet at 51.5 ppm. To confirm these results, we have acquired the ^{13}C NMR spectrum of [1′-^{13}C,1′-^{2}H]DMRL with simultaneous ^{1}H and ^{2}H decoupling (Figure 7C). This spectrum reveals a single peak at 51.5 ppm that confirms incorporation of deuterium at the C-1′ position. Thus, the reduction of the ribosylamino linkage to generate the product ribitylamino linkage catalyzed by RibD occurs via a hydride transfer step directly from NADPH to C-1′ of compound **3**.

The recently reported crystal structure of the *E. coli* enzyme complexed with the substrate analogue ribose 5-phosphate suggested that enzyme residue Asp 200 might act as a general base to deprotonate the amine group during catalysis. Asp 200 is close to the O-1 hydroxyl group from ribose 5-phosphate which corresponds to the predicted location of the amine group in the actual substrate, **3** (*19*). Therefore, we searched for indirect evidence of the involvement of a general base responsible for deprotonation of the amine that would be needed for the Schiff base mechanism. We have determined the pH dependence of the maximum velocity to probe the requirement for an enzyme base responsible for proton abstraction at the amine group. The k_{cat}−pH profile is very flat (Figure S2), with little dependence on pH (3-fold decrease between pH 5.5 and 9.2). While this does not preclude the requirement for a general base whose p*K* value is outside this range, it is supportive of a direct transfer mechanism. We have also determined the dependence of k_{cat} on solvent isotopic composition. Since hydride transfer is partially rate-limiting, as evidenced by the magnitude of ^{D}V, it seemed likely that a base-assisted deprotonation of the secondary amine might yield a nonunitary solvent kinetic isotope effect. However, the RibD reaction is insensitive to solvent isotopic composition (Figure S3), again providing indirect support for the direct hydride transfer mechanism. However, if one reconsiders the Schiff base mechanism and invokes a protonated iminium intermediate rather than the neutral imine drawn in Figure 2, then the requirement for general base-assisted deprotonation is removed and it is possible to reconcile our pH and solvent kinetic isotope effect results. We are at present considering experimental approaches to the unambiguous discrimination of these two mechanistic alternatives.

ACKNOWLEDGMENT

We thank Edward Nieves for performing mass spectroscopy experiments and Dr. Vern L. Schramm for kindly providing the enzymes HGPRTase and PRPPase.

SUPPORTING INFORMATION AVAILABLE

Reciprocal plots of INH−NADP versus NADPH and compound **3** (Figure S1), pH dependence of the maximum velocity (Figure S2), solvent kinetic isotope effects on the reaction (Figure S3), and enzymatic synthesis of [1′-^{13}C]GTP (Figure S4). This material is available free of charge via the Internet at http://pubs.acs.org.

REFERENCES

1. Massey, V. (2000) The chemical and biological versatility of riboflavin. *Biochem. Soc. Trans. 28*, 283–296.
2. Bacher, A., Eberhardt, S., Fischer, M., Kis, K., and Richter, G. (2000) Biosynthesis of vitamin b2 (riboflavin). *Annu. Rev. Nutr. 20*, 153–167.
3. Bacher, A., Eberhardt, S., Eisenreich, W., Fischer, M., Herz, S., Illarionov, B., Kis, K., and Richter, G. (2001) Biosynthesis of riboflavin. *Vitam. Horm. 61*, 1–49.
4. Burgess, C. M., Slotboom, D. J., Geertsma, E. R., Duurkens, R. H., Poolman, B., and van Sinderen, D. (2006) The riboflavin transporter RibU in *Lactococcus lactis*: Molecular characterization of gene expression and the transport mechanism. *J. Bacteriol. 188*, 2752–2760.
5. Duurkens, R. H., Tol, M. B., Geertsma, E. R., Permentier, H. P., and Slotboom, D. J. (2007) Flavin binding to the high affinity riboflavin transporter RibU. *J. Biol. Chem. 282*, 10380–10386.
6. Mac, L. J. (1952) The effects of certain purines and pyrimidines upon the production of riboflavin by *Eremothecium ashbyii*. *J. Bacteriol. 63*, 233–241.
7. Oltmanns, O., and Bacher, A. (1972) Biosynthesis of riboflavine in *Saccharomyces cerevisiae*: The role of genes rib 1 and rib 7. *J. Bacteriol. 110*, 818–822.
8. Bacher, A., and Lingens, F. (1971) Biosynthesis of riboflavin. Formation of 6-hydroxy-2,4,5-triaminopyrimidine in rib 7 mutants of *Saccharomyces cerevisiae*. *J. Biol. Chem. 246*, 7018–7022.
9. Bacher, A., and Lingens, F. (1970) Biosynthesis of riboflavin. Formation of 2,5-diamino-6-hydroxy-4-(1′-D-ribitylamino)pyrimidine in a riboflavin auxotroph. *J. Biol. Chem. 245*, 4647–4652.
10. Richter, G., Ritz, H., Katzenmeier, G., Volk, R., Kohnle, A., Lottspeich, F., Allendorf, D., and Bacher, A. (1993) Biosynthesis

of riboflavin: Cloning, sequencing, mapping, and expression of the gene coding for GTP cyclohydrolase II in *Escherichia coli*. *J. Bacteriol. 175*, 4045–4051.

11. Ritz, H., Schramek, N., Bracher, A., Herz, S., Eisenreich, W., Richter, G., and Bacher, A. (2001) Biosynthesis of riboflavin: Studies on the mechanism of GTP cyclohydrolase II. *J. Biol. Chem. 276*, 22273–22277.
12. Schramek, N., Bracher, A., and Bacher, A. (2001) Biosynthesis of riboflavin. Single turnover kinetic analysis of GTP cyclohydrolase II. *J. Biol. Chem. 276*, 44157–44162.
13. Ren, J., Kotaka, M., Lockyer, M., Lamb, H. K., Hawkins, A. R., and Stammers, D. K. (2005) GTP cyclohydrolase II structure and mechanism. *J. Biol. Chem. 280*, 36912–36919.
14. Richter, G., Fischer, M., Krieger, C., Eberhardt, S., Luttgen, H., Gerstenschlager, I., and Bacher, A. (1997) Biosynthesis of riboflavin: Characterization of the bifunctional deaminase-reductase of *Escherichia coli* and *Bacillus subtilis*. *J. Bacteriol. 179*, 2022–2028.
15. Burrows, R. B., and Brown, G. M. (1978) Presence of *Escherichia coli* of a deaminase and a reductase involved in biosynthesis of riboflavin. *J. Bacteriol. 136*, 657–667.
16. Hollander, I., and Brown, G. M. (1979) Biosynthesis of riboflavin: Reductase and deaminase of *Ashbya gossypii*. *Biochem. Biophys. Res. Commun. 89*, 759–763.
17. Nielsen, P., and Bacher, A. (1981) Biosynthesis of riboflavin. Characterization of the product of the deaminase. *Biochim. Biophys. Acta 662*, 312–317.
18. Fischer, M., Romisch, W., Saller, S., Illarionov, B., Richter, G., Rohdich, F., Eisenreich, W., and Bacher, A. (2004) Evolution of vitamin B2 biosynthesis: Structural and functional similarity between pyrimidine deaminases of eubacterial and plant origin. *J. Biol. Chem. 279*, 36299–36308.
19. Stenmark, P., Moche, M., Gurmu, D., and Nordlund, P. (2007) The crystal structure of the bifunctional deaminase/reductase RibD of the riboflavin biosynthetic pathway in *Escherichia coli*: Implications for the reductive mechanism. *J. Mol. Biol. 373*, 48–64.
20. Chen, S. C., Chang, Y. C., Lin, C. H., and Liaw, S. H. (2006) Crystal structure of a bifunctional deaminase and reductase from *Bacillus subtilis* involved in riboflavin biosynthesis. *J. Biol. Chem. 281*, 7605–7613.
21. Keller, P. J., Le Van, Q., Kim, S. U., Bown, D. H., Chen, H. C., Kohnle, A., Bacher, A., and Floss, H. G. (1988) Biosynthesis of riboflavin: Mechanism of formation of the ribitylamino linkage. *Biochemistry 27*, 1117–1120.
22. Bresler, S. E., Glazunov, E. A., Perumov, D. A., and Chernik, T. P. (1977) Riboflavin biosynthesis operon of *Bacillus subtilis*. XIII. Genetic and biochemical study of mutants with regard to intermediate stages of biosynthesis. *Genetika 13*, 2006–2016.
23. Mostad, S. B., Helming, H. L., Groom, C., and Glasfeld, A. (1997) The stereospecificity of hydrogen transfer to NAD(P)+ catalyzed by lactol dehydrogenases. *Biochem. Biophys. Res. Commun. 233*, 681–686.
24. Orr, G. A., and Blanchard, J. S. (1984) High-performance ion-exchange separation of oxidized and reduced nicotinamide adenine dinucleotides. *Anal. Biochem. 142*, 232–234.
25. Argyrou, A., Jin, L., Siconilfi-Baez, L., Angeletti, R. H., and Blanchard, J. S. (2006) Proteome-wide profiling of isoniazid targets in *Mycobacterium tuberculosis*. *Biochemistry 45*, 13947–13953.
26. Betts, L., Xiang, S., Short, S. A., Wolfenden, R., and Carter, C. W., Jr. (1994) Cytidine deaminase. The 2.3 Å crystal structure of an enzyme:transition-state analog complex. *J. Mol. Biol. 235*, 635–656.
27. Frick, L., Yang, C., Marquez, V. E., and Wolfenden, R. (1989) Binding of pyrimidin-2-one ribonucleoside by cytidine deaminase as the transition-state analogue 3,4-dihydrouridine and the contribution of the 4-hydroxyl group to its binding affinity. *Biochemistry 28*, 9423–9430.
28. Kati, W. M., and Wolfenden, R. (1989) Major enhancement of the affinity of an enzyme for a transition-state analog by a single hydroxyl group. *Science 243*, 1591–1593.
29. Kati, W. M., and Wolfenden, R. (1989) Contribution of a single hydroxyl group to transition-state discrimination by adenosine deaminase: Evidence for an "entropy trap" mechanism. *Biochemistry 28*, 7919–7927.
30. Kati, W. M., Acheson, S. A., and Wolfenden, R. (1992) A transition state in pieces: Major contributions of entropic effects to ligand binding by adenosine deaminase. *Biochemistry 31*, 7356–7366.
31. Fierke, C. A., Johnson, K. A., and Benkovic, S. J. (1987) Construction and evaluation of the kinetic scheme associated with dihydrofolate reductase from *Escherichia coli*. *Biochemistry 26*, 4085–4092.
32. Miller, G. P., and Benkovic, S. J. (1998) Stretching exercises: Flexibility in dihydrofolate reductase catalysis. *Chem. Biol. 5*, R105–R113.
33. Yu, M., Magalhaes, M. L., Cook, P. F., and Blanchard, J. S. (2006) Bisubstrate inhibition: Theory and application to N-acetyltransferases. *Biochemistry 45*, 14788–14794.
34. Magalhaes, M. L., Vetting, M. W., Gao, F., Freiburger, L., Auclair, K., and Blanchard, J. S. (2008) Kinetic and structural analysis of bisubstrate inhibition of the *Salmonella enterica* aminoglycoside 6′-N-acetyltransferase. *Biochemistry 47*, 579–584.
35. Morrison, J. F., and Stone, S. R. (1988) Mechanism of the reaction catalyzed by dihydrofolate reductase from *Escherichia coli*: pH and deuterium isotope effects with NADPH as the variable substrate. *Biochemistry 27*, 5499–5506.
36. Le Van, Q., Keller, P. J., Bown, D. H., Floss, H. G., and Bacher, A. (1985) Biosynthesis of riboflavin in *Bacillus subtilis*: Origin of the four-carbon moiety. *J. Bacteriol. 162*, 1280–1284.

BI800264G